Influence of Orientational Fluctuations on Electron Transfer in Systems of Donor–Acceptor Pairs

R. P. Domingue and M. D. Fayer*

Department of Chemistry, Stanford University, Stanford, California 94305 *(Received: April 7, 1986)*

We present model calculations on the influence of fluctuations in the relative orientation of a donor and acceptor pair held at fixed separation on electron-transfer observables. A simple model of the angular dependence of the transfer rate based on the overlap of a S orbital with a P orbital is used, and a variety of angular fluctuation distribution functions are employed. The effect on observables is calculated for electron transfer which is fast relative to the fluctuations and which is slow relative to the fluctuations. It is demonstrated that the extent and geometry of the fluctuations can have a significant effect on electron transfer even though the donor and acceptor are held at fixed separation.

I. Introduction

An understanding of the complex phenomenon of donor to acceptor electron transfer has long been considered of fundamental importance both to basic research and applied science.[1,2] Long-range electron transfer can occur via a quantum mechanical tunneling mechanism where the donor and acceptor states maintain their integrity. Many physically important processes involve electron transfer from a photoexcited donor to an acceptor. Photoinduced electron transfer follows initial excitation of the donor from the ground state to an excited state. The transfer is due to the weak coupling between the donor state and the acceptor state. This transfer can be described with Fermi's golden rule, with the transfer rate between a single donor and acceptor pair in a fixed configuration given by[3-5]

$$n(R,\theta) = \frac{2\pi}{\hbar}(\mathrm{FC})|T_{\mathrm{DA}}|^2 \qquad (1)$$

FC is the Franck-Condon factor and T_{DA} is the electron-transfer matrix element. The influence of the angular dependence of the transfer rate on experimental observables will be the focus of this paper.

It has been demonstrated[6,7] that T_{DA} is proportional to the overlap of the donor highest occupied molecular orbital and the acceptor lowest unoccupied molecular orbital.[3] In general, the overlap integral will be dependent on the distance and relative orientations of the orbitals. A number of investigators have studied the distance and angular dependence of the electron-transfer rate theoretically and experimentally. The systems studied included donors and acceptors randomly distributed in a glass,[8-10] a donor and an acceptor linked by a rigid saturated hydrocarbon chain,[11,12] and a donor and an acceptor held fixed in a protein.[13-15] These systems have been analyzed experimentally by looking at the time-dependent and steady-state luminescence quenching. A number of theoretical approaches have been used within the golden rule framework.[4,6,10]

When electron transfer between a pair of molecules at fixed separation and orientation is considered, it has been recognized that the orientational dependence of the transfer rate is important.[6,10] Since molecules are spatially anisotropic, at fixed separation the donor–acceptor overlap will be a function of the relative orientation of the molecules. The dependence of the transfer rate on both distance and orientation can make it experimentally difficult to separate the angular and spatial influence on observables. Frequently the angular dependence has been excluded from data analysis. For molecular donor and acceptor systems, one must know the particular form of the overlap orientational dependence. In addition one must know the donor–acceptor relative orientation as well as the distance-dependent parameters in order to predict the transfer rate for a given donor–acceptor separation.

At finite temperatures the relative orientations between donors and acceptors can fluctuate about their equilibrium values. Here we consider the effect a restricted set of relative orientations will have on time-resolved fluorescence quenching produced by electron transfer for an ensemble of systems of a donor separated by a fixed distance from an acceptor. A particular form of the angular dependence of the electron-transfer rate is used to illustrate the nature of the phenomena.

In a previous paper,[10] it has been shown that for an S orbital interacting with a P orbital a distance R away, the effect on the decay curves for various fixed relative orientations can be quite dramatic. Here the effect on decay curves for a number of different types of restricted sets of relative orientations is examined. The curves are calculated in the limit of very fast reorientational motion with respect to the electron-transfer rate, and they are calculated in the limit of very slow reorientational motion with respect to the electron-transfer rate. The first case corresponds to torsional or librational motion or very rapid isomerization that affects relative angles but not distances. The second case corresponds to essentially fixed relative orientation between a donor–acceptor pair for a sample in which there is a distribution of pair relative orientations. It is demonstrated that the nature of the angular distribution function can have a significant effect on electron-transfer observables, even though the donor–acceptor pair separation is fixed.

II. Models and Calculations

In this section a series of calculations are presented that describe the combined effects of orientation and distance on electron transfer in an ensemble of systems of one donor and one acceptor separated by a distance R. An S-orbital P-orbital overlap model is used to illustrate the effects of restricted relative orientations on the electron-transfer decay curve. While this is a simple model,

(1) Miller, J. R.; Beitz, J. V.; Huddleston, R. K. *J. Am. Chem. Soc.* **1984**, *106*, 5057.
(2) Fendler, J. H. *J. Phys. Chem.* **1985**, *89*, 2730.
(3) Dexter, D. L. *J. Chem. Phys.* **1953**, *21*, 836.
(4) Siders, P.; Cave, R. J.; Marcus, R. A. *J. Chem. Phys.* **1984**, *81*, 5613.
(5) Kestner, N. R.; Logan, J.; Jortner, J. *J. Phys. Chem.* **1974**, *78*, 2148.
(6) Brocklehurst, B. *J. Phys. Chem.* **1979**, *83*, 536.
(7) Magee, J. L. *J. Chem. Phys.* **1940**, *8*, 687.
(8) Miller, J. R.; Beitz, J. V. *J. Chem. Phys.* **1981**, *74*, 6746.
(9) Namiki, A.; Nakashima, N.; Yoshihara, K. *J. Chem. Phys.* **1979**, *71*, 925.
(10) Domingue, R. P.; Fayer, M. D. *J. Chem. Phys.* **1985**, *83*, 2242.
(11) Miller, J. R.; Calcaterra, L. T.; Closs, G. L. *J. Am. Chem. Soc.* **1984**, *106*, 3047.
(12) Hush, N. S.; Paddon-Row, M. N.; Cotsaris, E.; Oevering, H.; Verhoeven, J. W.; Heppener, M. *Chem. Phys. Lett.* **1985**, *117*, 8.
(13) Nocera, D. G.; Winkler, J. R.; Yocom, K. M.; Bordignon, E.; Gray, H. B. *J. Am. Chem. Soc.* **1984**, *106*, 5145.
(14) Simolo, K. P.; McLenden, G. L.; Mauk, M. R.; Mauk, A. G. *J. Am. Chem. Soc.* **1984**, *106*, 5012.
(15) McGounty, J. M.; Blough, N. V.; Hoffman, B. M. *J. Am. Chem. Soc.* **1983**, *105*, 4470.

0022-3654/86/2090-5141$01.50/0

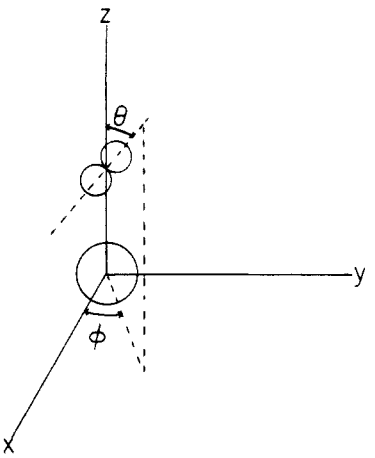

Figure 1. Coordinate system and variables for the SP calculations. An S orbital with positive sign is situated at the origin. A P orbital with azimuthal angle θ and polar angle ϕ is displaced a distance R along the z axis.

it is sufficient to illustrate the nature of the effects.

Suppose that at time $t = 0$ an ensemble of dilute donors is excited. In the absence of acceptors, the probability of finding the excitation on the donor at time t, $\rho(t)$, decays exponentially with the excited-state lifetime τ_0; i.e., $\rho(t) = \exp(-t/\tau_0)$. The excited-state radiative decay results in fluorescence or phosphorescence depending upon whether the initial excited state is a singlet or a triplet. When the acceptor is present, the probability decays more rapidly due to the addition of the electron-transfer pathway for quenching of the electronic excited state. If $n(R,\theta)$ is the transfer rate from a donor D to an acceptor A at the distance R and relative orientations described by θ, then the time-dependent probability that the donor is excited is determined by the probability that the donor decays with the lifetime τ_0 times the probability that an electron transfers to the acceptor, namely

$$\rho(t) = \exp[-t/\tau_0 - tn(R,\theta)] \tag{2}$$

This probability is then ensemble averaged over the distribution of donor–acceptor configurations to give the emission decay curve, which can be measured by performing a fluorescence quenching experiment. For the case of a donor and an acceptor held at a fixed distance R, the emission decay curve is found by averaging over the set of orientations described by θ.

Consider the electron-transfer rate $n(R,\theta)$. For the model presented here, there is a 2S orbital on molecule 1 and a 2P orbital of molecule 2 separated by a distance R. The schematic for this system is shown in Figure 1. If ψ_1 is the 2S orbital on molecule 1, then $\psi_2 = P_{2x} \sin\theta\cos\phi + P_{2y} \sin\theta \sin\phi + P_{2z} \cos\theta$ is the 2P orbital, expressed in terms of the P_x, P_y, and P_z components, on molecule 2. From this geometry it is readily established that the overlap between the ψ_1 and the ψ_2 orbitals, S_{12}, is given by

$$S_{12} = S(2s,2p_\pi) \sin\theta\cos\phi + S(2s,2p_\pi) \sin\theta \sin\phi - S(2s,2p_\sigma) \cos\theta \tag{3}$$

Since $S(2s,2p_\pi) = 0$ due to orthogonality

$$S_{12} = -\cos\theta S(2s,2p_\sigma) \tag{4}$$

From Mulliken's 1949 table of overlap integrals[16]

$$S(2s,2p_\sigma) = \frac{3^{1/2}}{6}\left[p + p^2 + \left(\frac{7}{15}\right)p^3 + \left(\frac{2}{15}\right)p^4\right]e^{-p} \tag{5}$$

$p = R/2a_0$, where a_0 is the Bohr radius. As usual, we replace the polynomial in R times the exponential by a new exponential with a modified Bohr radius, a. The substitution is justified since the polynomial times the exponential is well approximated by an exponential with a different decay constant for the distances of interest here. This gives an overlap function of $S_{12}(R,\theta) = -\cos\theta e^{-R/2a}$, which yields a final form for the transfer rate of

$$n(R,\theta) = \frac{3}{\tau_0}\cos^2\theta \exp[\gamma(1 - R/R_0)] \tag{6}$$

where $\gamma = R_0/a$ and R_0 is the critical transfer distance. R_0 is the distance at which an excited donor has equal probability of decaying to the ground state or transferring an electron to an acceptor. R_0 is defined in terms of the angle-averaged transfer rate.

The lifetime contribution can be factored out of the problem and only the electron-transfer contribution, ET, will be discussed further. There are two limiting cases that are addressed. The first is the limit that the transfer rate is much faster than the reorientation rate. In this case we must angle average the observable over the distribution of fixed angles of the donor–acceptor pairs. The second case is the limit that the transfer rate is much slower than the reorientation rate. Here we must angle average the transfer rate and use this averaged transfer rate in the exponential expression.

A number of different types of restricted orientational distributions are considered. These include motion in a cone and motion in a plane. Uniform angular probability with a sharp angular cutoff and Gaussian angular probabilities are employed. A general description of how the angle averages are performed for any model is presented. Then the model of uniform motion in a cone for both fast transfer relative to reorientation rate and slow transfer relative to reorientation rate is derived. The derivations of the other models are presented in the Appendix. Note that we only need to average over rotations of the molecule with the P orbital, since the transfer rate is invariant to rotations of the S orbital.

If the transfer rate is much faster than the rate of reorientation, then we must average over the exponential, namely

$$\langle \mathrm{ET}(t)\rangle \equiv \frac{\int_\phi\int_\theta e^{-tn(R,\theta)}\, P(\theta,\phi)\, d\theta\, d\phi}{\int_\phi\int_\theta P(\theta,\phi)\, d\theta\, d\phi} \tag{7}$$

where $P(\theta,\phi)$ is the probability of finding the P orbital oriented with spherical angles θ and ϕ in space. The limits of integration are used to restrict the angular distribution for the cases in which there are sharp angular cut-offs. Two types of conical models are used

$$P(\theta,\phi) = \sin\theta \qquad \text{cone} \tag{8}$$

and

$$P(\theta,\phi) = e^{-\theta^2/2\sigma^2}\sin\theta \qquad \text{Gaussian cone} \tag{9}$$

σ is the standard derivation for the Gaussian centered at $\theta = 0°$.

If the transfer rate is much slower than the rate of reorientation, then we must first average over the transfer rate; we can then use this transfer rate in the exponential, namely

$$\langle n(R)\rangle = \frac{\int_\phi\int_\theta n(R,\theta)\, P(\theta,\phi)\, d\theta\, d\phi}{\int_\phi\int_\theta P(\theta,\phi)\, d\theta\, d\phi} \tag{10}$$

This gives

$$\langle \mathrm{ET}(t)\rangle = e^{-t\langle n(R)\rangle} \tag{11}$$

In the first model (cone), the positive lobe of the P orbital can move anywhere on a spherical surface restricted by the angles $\theta = \theta_0$ to $\theta = \theta_1$ (see Figure 1). For the transfer rate much faster than the reorientation rate

$$\langle \mathrm{ET}(t)\rangle = \frac{\int_{\theta_0}^{\theta_1} e^{-(3t/\tau_0)\cos^2\theta(e^{\gamma(1-R/R0)}} \sin\theta\, d\theta}{\int_{\theta_0}^{\theta_1}\sin\theta\, d\theta} \tag{12}$$

The integral in the numerator is performed numerically. This model is called uniform motion on a conic spherical section if θ_0

(16) Mulliken, R. S.; Rieke, C. A.; Orloff, D.; Orloff, H. *J. Chem. Phys.* **1949**, *17*, 1248.

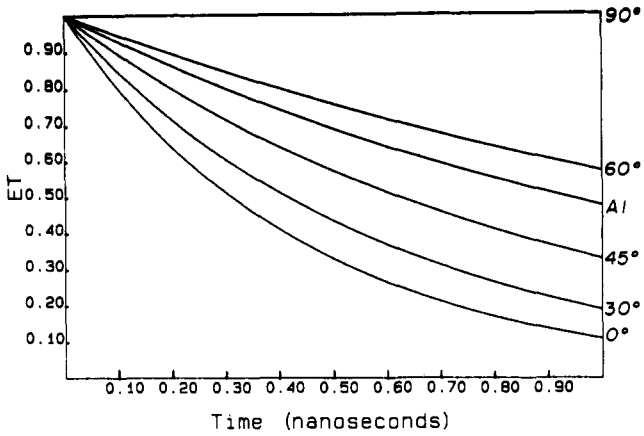

Figure 2. Electron-transfer decay curves for angle-independent (AI) and fixed SP angle-dependent calculations. The angle label by each curve indicates the relative orientation of the P orbital. Note that there is no transfer for 90°. The experimental decay curves would be obtained by multiplying by the lifetime decay. Note the large variation in decay rates with relative orientation. The angle-independent transfer rate, frequently employed in experimental analysis, is clearly not appropriate when there is a strong angular dependence to the transfer rate. The parameters are R = 8 Å, R_0 = 10 Å, a = 1 Å, and τ_0 = 10 ns.

= 0. For the limit that the transition rate is much slower than the orientation time

$$\langle \mathrm{ET}(t) \rangle = \exp\left[-t \frac{\int_{\theta_0}^{\theta_1} (3/\tau_0) \cos^2\theta (e^{-\gamma(1-R/R_0)}) \sin\theta \, d\theta}{\int_{\theta_0}^{\theta_1} \sin\theta \, d\theta} \right] \quad (13)$$

which yields

$$\langle \mathrm{ET}(t) \rangle = \exp\left[-\frac{t}{\tau_0} e^{\gamma(1-R/R_0)} (\cos^2\theta_0 + \cos\theta_0 \cos\theta_1 + \cos^2\theta_1) \right] \quad (14)$$

The other models are derived in the Appendix. These include motion on a conic spherical section with a Gaussian probability density and uniform and Gaussian-modified motion of the P orbital in the plane of the two orbitals. In the uniform models, there is equal probability of any orientation between the cut-off limits. In the Gaussian models, there is a Gaussian probability distribution of orientations with standard deviation, σ.

Figure 2 shows some plots of the electron-transfer decay function ET vs. time for an S orbital and a P orbital separated by the distance R. The parameters for all of the plots are R = 8 Å, R_0 = 10 Å, a = 1 Å, and τ_0 = 10 ns. The curve labeled AI is the curve for an angle-independent transfer rate, i.e., $n(R) = 1/\tau_0 \exp[\gamma(1 - R/R_0)]$, which is commonly employed. The curves labeled 0°, 30°, 45°, and 90° are for fixed S and P orientations with the transfer rate of eq 6, where the angle is the angle that the P orbital makes with the z axis. The experimental emission decay observable is obtained by multiplying these curves by the lifetime contribution $\exp(-t/\tau_0)$. There is no motion in this model, but it is clear that an angular dependence of the transfer rate can have a marked effect on the emission decay. Notice that the fastest decay occurs when the P orbital points directly toward the S orbitals. When the two orbitals are orthogonal, θ = 90°, there is no overlap and hence no electron transfer. The particular choice of parameters and time scales for this figure and the following figures was made to clearly demonstrate the phenomena. None of the arguments are dependent on the particular choice of parameters.

Figure 3 shows a number of plots of the electron-transfer decay function ET vs. time. In this model the transfer is between an S and P orbital separated by a distance R where the positive lobe of the P orbital is restricted to be on the spherical surface section intersected by a cone. The probability of finding the positive lobe of the P orbital anywhere on this spherical surface section is

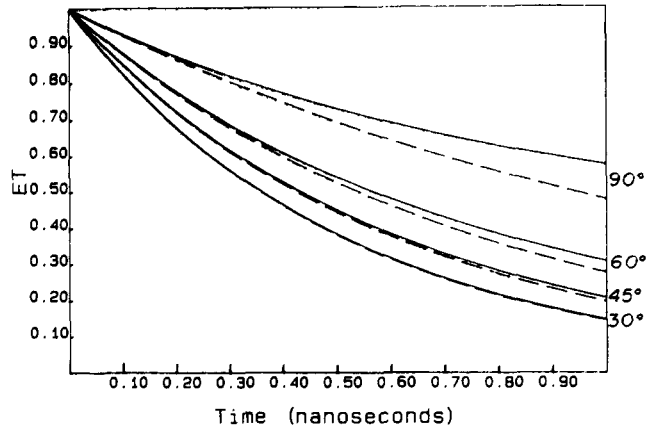

Figure 3. Electron-transfer decay curves for SP angle-dependent calculations. The positive lobe of the P orbital is restricted to lie on the section of the surface of a sphere intersected by a cone whose vertex is at the center of the sphere. The solid curves are for transfer fast compared to the angular fluctuations, and the dashed curves are for transfer slow compared to the angular fluctuations. The angle label next to each pair of curves is the half-angle of the cone of fluctuations. As the fluctuations increase, the curves decay more slowly and the differences between the curves, the dashed and the solid curves, increases. The parameters are R = 8 Å, R_0 = 10 Å, a = 1 Å, and τ_0 = 10 ns.

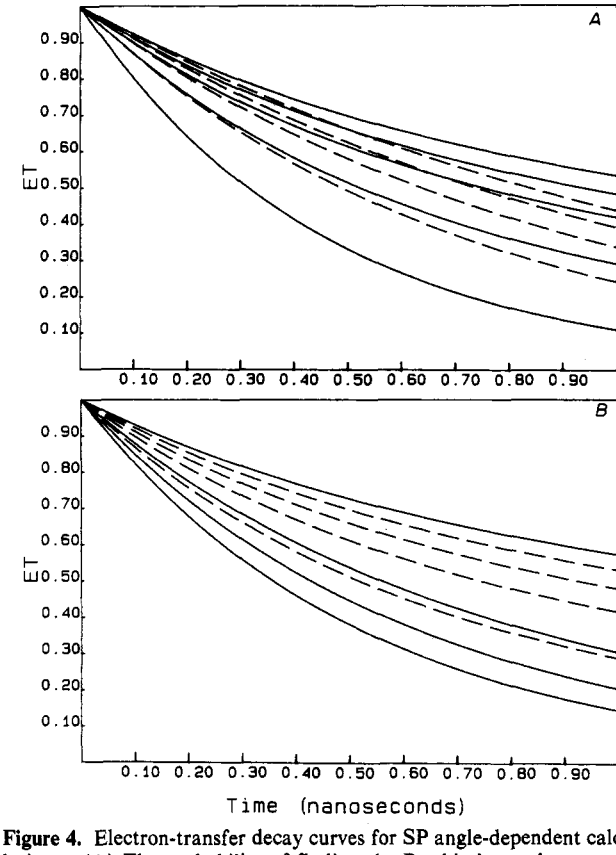

Figure 4. Electron-transfer decay curves for SP angle-dependent calculations. (A) The probability of finding the P orbital anywhere on the spherical surface is given by a Gaussian distribution centered at θ = 0°. The solid curves are for transfer fast compared to the angular fluctuations, and the dashed curves are for transfer slow compared to the angular fluctuations. Both the solid and dashed curves are for a Gaussian standard deviation, σ, from top to bottom as follows: 90°, 60°, 45°, 30°, 2°. It is seen that the relative rate of electron transfer to angular fluctuations can significantly affect the decay curves. (B) A comparison of transfer fast relative to angular fluctuations for the model of Figure 3 and Figure 4A. The solid curves are for the uniform distribution model while the dashed curves are for the Gaussian distribution model. The curves are from top to bottom as follows: 90°, 60°, 45°, 30°. It is seen that the shape of the decay curves are dependent on the type of restriction on the motion, i.e., uniform distribution with a sharp cutoff or Gaussian distribution with restrictive standard deviations. The parameters are R = 8 Å, R_0 = 10 Å, a = 1 Å, and τ_0 = 10 ns.

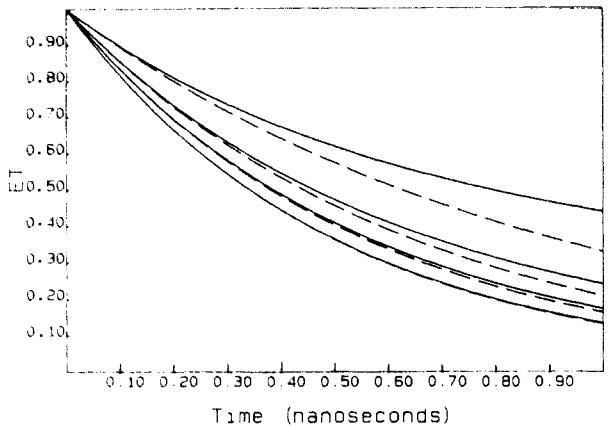

Figure 5. Electron-transfer decay curves for SP angle-dependent calculations. The positive lobe of the P orbital is restricted to lie in a plane with equal angular deviations on either side of $\theta = 0°$. The solid curves are for transfer fast compared to the angular fluctuations, and the dashed curves are for transfer slow compared to the angular fluctuations. The curves, from top to bottom, are for ±90°, ±60°, ±45°, and ±30° excursions. As in Figure 3, the solid curves decay more slowly than the dashed curves, and this difference increases as the extent of fluctuation increases. Again the relative rates of transfer and angular fluctuation can affect the shape of the decay curves. The parameters are $R = 8$ Å, $R_0 = 10$ Å, $a = 1$ Å, and $\tau_0 = 10$ ns.

uniformly distributed. The size of the cone is labeled by 30°, 45°, 60°, or 90°, which is the restriction on the largest angle the P orbital can make with the z axis. In Figure 3 the solid curves are for a transfer rate that is much faster than the reorientation rate and the observable must be averaged. Equation 12 is used. The dashed curves are for a transfer rate that is much slower than the reorientation rate, and the transfer rate must first be averaged. Equation 14 is used. As expected the curves in Figure 2 differ considerably from the curves in Figure 3. This is most noticeably apparent in the curves that cover the hemispherical section. What is especially interesting is that, as shown in Figure 3, the limits of fast and slow transfer with respect to the reorientation rate show distinct differences for the larger spherical sections. However, for smaller angular variation, the fast and slow cases are essentially indistinguishable. Transfer that is on the same time scale as the reorientation would produce curves that lie between the fast and slow cases.

Figure 4 shows a number of plots of the electron-transfer decay function ET vs. time for the model that allows the positive lobe of the P orbital to extend over the entire hemispherical surface. However, the probability of finding the positive lobe anywhere in space is not uniform but is determined by a Gaussian centered at $\theta = 0°$. The standard deviation, σ, for both the solid and dashed curves are, from top to bottom, 90°, 60°, 45°, 30°, and 2°. For $\theta = 2°$ the positive lobe of the P orbital is mainly around $\theta = 0°$ so that this curve is nearly identical with the $\theta = 0°$ curve of Figure 2. As σ becomes larger the motion is less restricted and the decays slow down. The solid curves in Figure 4A are for the case in which the transfer rate is much faster than the reorientation rate. These curves are calculated from eq A1. The dashed curves in Figure 4A are for the case in which the transfer rate is much slower than the reorientation rate. These curves are calculated from eq A2. It is clear that the rate of transfer relative to the rate of angular fluctuation has a significant effect on the decays. Figure 4B compares the fast transfer rate cases of the uniform probability distribution and the Gaussian probability distribution. The solid curves are for the uniform probability distributions of Figure 3. The dashed curves are for the Gaussian distributions of Figure 4A. If one compares the uniform model with cutoff at say 45° to the Gaussian model with $\sigma = 45°$, the uniform model is more restrictive and hence the curves decay more rapidly.

Figure 5 shows plots of the electron-transfer decay function ET vs. time for a different type of orientation restriction. In this model the P orbital is restricted to move in a plane containing the S and P orbitals. The solid curves are for the case when the

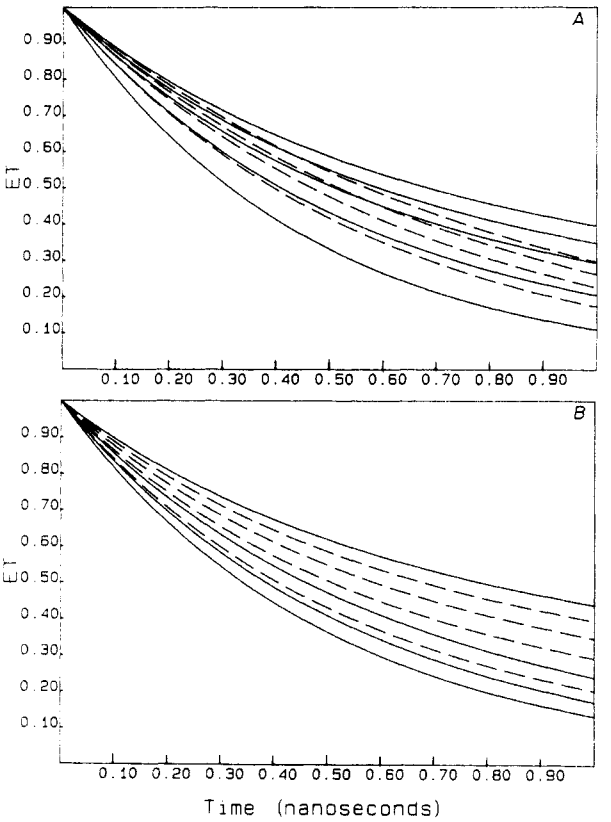

Figure 6. Electron-transfer decay curves for SP angle-dependent calculations. (A) The positive lobe of the P orbital is restricted to lie on a plane with equal angular deviations on either side of $\theta = 0°$. The probability is given by a Gaussian distribution centered around $\theta = 0°$. The solid curves are for transfer faster than angular fluctuations, and the dashed curves are for transfer slower than angular fluctuations. The fluctuations are restricted by specifying the standard deviation, σ. The curves from top to bottom have σ equal to 90°, 45°, 30°, and 2°. Notice the differences in the shapes of the solid and dashed decay curves and that for the same σ the solid curve has a slower decay than the dashed curve. Again, as in the cone model, the relative rates of transfer and angular fluctuation change the shape of the decay curves. (B) Comparison of uniform to Gaussian plane model for the transfer rate faster than the angular fluctuation rate. The uniform model curves are the solid curves while the Gaussian model curves are the dashed curves. The uniform curves are from top to bottom ±90°, ±60°, ±45°, and ±30°. The Gaussian curves are from top to bottom σ = 90°, 60°, 45°, and 30°. Notice that even for the same geometrical motion (i.e., motion in a plane) the type of motion (i.e., sharp cutoff or Gaussian distribution) can affect the shape of the decay curves. The parameters are $R = 8$ Å, $R_0 = 10$ Å, $a = 1$ Å, and $\tau_0 = 10$ ns.

transfer rate is much faster than the reorientation rate. The curves for this figure are calculated from eq A4. The dashed curves are for the case where the transfer rate is much slower than the reorientation rate. The curves of this figure are calculated from eq A6. The restrictions on the motion are, from top to bottom, ± 90°, ± 60°, ± 45°, and ± 30°, all measured from the z axis. The trends in this model are similar to the behavior of the uniform cone model. For large angular deviations, the fast and slow cases are quite different, while for smaller angular deviations the curves become indistinguishable.

Figure 6A shows a number of plots of the electron-transfer decay function ET vs. time for the Gaussian planar model; i.e., the probability of finding the positive lobe of the P orbital is given by a Gaussian centered on the z axis. In the figure the positive lobe can move over the upper half plane and the standard deviations of the Gaussian, σ, are 90°, 60°, 45°, 30°, and 2°, from top to bottom. As expected the $\sigma = 2°$ curve is nearly identical with the 0° curve of Figure 2 and the $\sigma = 2°$ of Figure 4. The solid curves in Figure 6A are for a transfer rate that is much faster than the reorientation rate (eq A7). The dashed curves are for a transfer rate that is much slower than the reorientation rate (eq A8). Figure 6B shows a comparison for the fast transfer cases

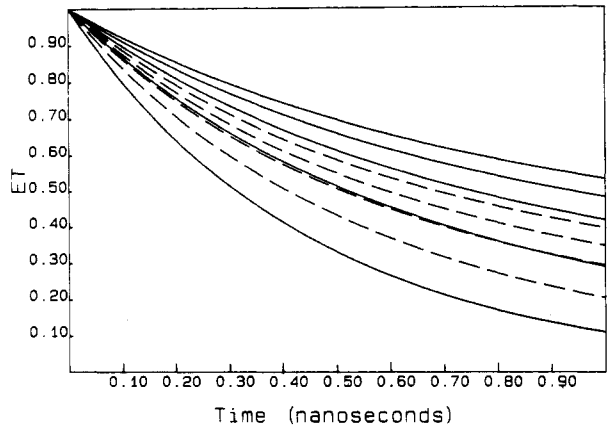

Figure 7. Electron-transfer decay curves for SP angle-dependent calculations. A comparison of the Gaussian cone model of Figure 4A with the Gaussian plane model of Figure 6A. The transfer rate is faster than the angular fluctuation rate. The cones (solid) and planes (dashed) have (from top to bottom) the standard deviations 90°, 60°, 45°, 30°, and 2°. In this figure curves with the same standard deviations but different geometrical motion (cones vs. planes) have different decay curves. The parameters are R = 8 Å, R_0 = 10 Å, a = 1 Å, and τ_0 = 10 ns.

of Figure 5A and Figure 6A. The solid curves are for planes with a uniform probability distribution and the dashed curves are for a Gaussian probability distribution. As in the cone model, the Gaussian and the uniform distribution curves are markedly different, demonstrating that different kinds of angular distributions are manifested in the decay curves, even when the geometries of the distributions (planes or cones) are the same.

Figure 7 shows some comparisons between the cone model (solid line) and the planar model (dashed lines). The curves are for the Gaussian angular distribution and the transfer rate is fast relative to the reorientation rate. This figure shows that given the same type of angular distribution, the geometry (plane, cone) of the distribution can have a profound effect on the electron-transfer observables. While particular models of angular distributions and spatial geometries of the motion have been employed, the types of effects illustrated here will occur for many other physical situations.

III. Discussion and Conclusions

This paper has focused on the effects of an angle-dependent electron-transfer rate on the time-resolved emission observable for an ensemble of systems of one donor and one acceptor at fixed distance. For simplicity an SP angular-dependent transfer rate model was used. The central issue that has been addressed is the influence of fluctuations in the relative orientation of the donor–acceptor pair on through space electron transfer. Electron transfer fast and slow relative to the time scale of the angular fluctuations has been considered. From the results it is clear that orientational fluctuations can have dramatic effects on the time-resolved electron-transport observables. The type of orientational fluctuations in the models, motion in a plane or cone, can result in quite different decay curves. In addition we have shown that the electron-transfer observables are sensitive to whether the electron transfer is fast or slow relative to the reorientational motions.

The materials in this paper points out the influences of angular fluctuation on what otherwise can be a very well-defined experimental system, i.e., a donor and acceptor pair separated by a known distance R. To study the distance dependence of through space electron transfer (as opposed to transfer that is essentially through bonds linking a donor and acceptor) it is not only necessary to space the donor–acceptor pair at various distances, but it is also necessary to maintain the relative orientations and the fluctuations in the relative orientations. In other contexts, understanding of electron transfer involves more than the distance and angles but also involves the fluctuations in the relative orientations. For example, an observed temperature dependence in electron transfer between donor–acceptor pairs could, in part, be due to a temperature dependence of the orientational fluctuations.

Acknowledgment. This work was supported by the Department of Energy, Office of Basic Energy Sciences (Grant No. DE-FG03-84ER13251).

Appendix

In this appendix we derive expressions for the several types of models presented in the figures of section II. The different types of models involve using the SP angular-dependent electron-transfer rate then averaging over a restricted set of angles. The models are presented with two basic types of orientation restrictions. The first is for a uniform probability distribution of orientations over a restricted set of angles. The second is for a Gaussian-modified probability distribution of orientations centered on the z axis. Here the orientations were allowed to span all space, but a variation in the Gaussian standard deviation effectively causes some orientations to be sampled more frequently than others. In addition, the averages are performed in two distinct limits. The first limit is a transfer rate that is much faster than the reorientation rate, and the observable must be angle averaged. The second limit is a transfer rate that is much slower than the reorientational rate, and the transfer rate must be averaged.

The first model is a P orbital restricted to move on the spherical section intersected by a cone. Equation 12 gives the results for uniform motion in a cone for the limit of fast transfer rate relative to reorientation rate. Equation 14 gives the results for uniform motion in a cone for the limit of slow transfer rate relative to reorientation rate. If the probability distribution is given by a Gaussian, then combining eq 7 and 9 gives

$$\langle \mathrm{ET}(t) \rangle = \frac{\int_{\theta_0}^{\theta_1} e^{-(3t/\tau_0)\cos^2\theta(e^{\gamma(1-R/R_0)})}\, e^{-\theta^2/(2\sigma^2)} \sin\theta\, \mathrm{d}\theta}{\int_{\theta_0}^{\theta_1} e^{-\theta^2/(2\sigma^2)} \sin\theta\, \mathrm{d}\theta} \tag{A1}$$

Both numerator and denominator are evaluated numerically. In the figures θ_0 was chosen as 0° and θ_1 was chosen as 90°. In this manner σ could be varied to make the Gaussian narrow or broad.

Equations 10 and 11 are also modified by eq 9. This angle average is for the limit in which the transfer rate is much slower than the reorientation rate. This gives

$$\langle \mathrm{ET}(t) \rangle = \exp\left[-t \frac{\int_{\theta_0}^{\theta_1} (3/\tau_0) \cos^2\theta(e^{\gamma(1-R/R_0)}) e^{-\theta^2/(2\sigma^2)} \sin\theta\, \mathrm{d}\theta}{\int_{\theta_0}^{\theta_1} \epsilon^{-\theta^2/(2\sigma^2)} \sin\theta \mathrm{d}\theta} \right] \tag{A2}$$

Again the numerator and denominator are numerically integrated between the limits θ_0 = 0° and θ_1 = 90° where σ is varied.

The second model describes restricted motion of the P orbital in a plane. In this model the probability distribution for uniform motion is

$$P(\theta,\phi) = 1 \tag{A3}$$

With this distribution, the limit in which the transfer rate is fast relative to the reorientation time becomes

$$\langle \mathrm{ET}(t) \rangle = \frac{\int_{\theta_0}^{\theta_1} e^{-3(t/\tau_0)\cos^2\theta(e^{\gamma(1-R/R_0)})}\, \mathrm{d}\theta}{\int_{\theta_0}^{\theta_1} \mathrm{d}\theta} \tag{A4}$$

The numerator is evaluated numerically. This model allows uniform motion between any two angles in the plane. The intervals in Figure 5 are chosen to be symmetric around θ = 0°.

The other limit, in which the transfer rate is much slower than the reorientation rate, is expressed as follows:

$$\langle \mathrm{ET}(t) \rangle = \exp\left[-t \frac{\int_{\theta_0}^{\theta_1} (3/\tau_0) \cos^2\theta(e^{\gamma(1-R/R_0)})\, \mathrm{d}\theta}{\int_{\theta_0}^{\theta_1} \mathrm{d}\theta} \right] \tag{A5}$$

After the integration and algebra are done, this reduces to

$$\langle ET(t)\rangle = \exp\left[-\frac{3t}{2\tau_0}\left(1 + \frac{\sin 2\theta_1 - \sin 2\theta_0}{2(\theta_1 - \theta_0)}\right)e^{\gamma(1-R/R_0)}\right] \tag{A6}$$

This function is calculated and plotted in Figure 5 with the limits chosen to be symmetric about $\theta = 0°$.

If eq A4 is modified by a Gaussian probability distribution centered about $\theta = 0°$, then it becomes

$$\langle ET(t)\rangle = \frac{\int_{\theta_0}^{\theta_1} \epsilon^{-(3t/\tau_0)\cos^2\theta(e^{\gamma(1-R/R_0)})} e^{-\theta^2/(2\sigma^2)}\, d\theta}{\int_{\theta_0}^{\theta_1} e^{-\theta^2/(2\sigma^2)}\, d\theta} \tag{A7}$$

Both denominator and numerator are evaluated numerically for convenience. This is the fast transfer rate relative to reorientation rate limit, where θ_0 is $-90°$ and θ_1 to $90°$, chosen so that all space is spanned. The orientation restriction is achieved by varying σ to make the Gaussian narrow or broad.

The final limiting case is for motion in a plane with a Gaussian angular distribution where the transfer rate is slow relative to the reorientational rate. For this case $\langle ET(t)\rangle$ becomes

$$\langle ET(t)\rangle = \exp\left[-t\frac{\int_{\theta_0}^{\theta_1} (3/\tau_0)\cos^2\theta(e^{\gamma(1-R/R_0)}) e^{-\theta^2/(2\sigma^2)}\, d\theta}{\int_{\theta_0}^{\theta_1} e^{-\theta^2/(2\sigma^2)}\, d\theta}\right] \tag{A8}$$

For convenience these integrals were numerically evaluated. Again, the curves in Figure 6 were calculated for a symmetric interval, $\theta_0 = -90°$ and $\theta_1 = 90°$, with σ varying to give orientation restrictions.